



Delineation of groundwater potential areas using RS/GIS and geophysical methods: a case study from the western part of Iran

Davoud Bagheri¹ · Abdollah Taheri Tizro¹ · Saeid Okhravi² · Alan Fryar³ · Nerantzis Kazakis⁴ · Konstantinos Voudouris^{4,5}

Received: 23 February 2021 / Accepted: 1 September 2022 / Published online: 21 October 2022
© Saudi Society for Geosciences 2022

Abstract

Groundwater potential maps constitute a valuable tool for groundwater sustainable management in arid regions. In this study, a groundwater potential map was developed for the Asadabad plain (Iran). The method deployed remote sensing techniques and hierarchical analysis, while geoelectric data were used to verify the results of the study. The methodology used extracted information from thematic maps including lithology, the density of lineaments, drainage density, topography, slope, slope aspect, land use, distance from streams, distance from lineaments, rainfall, and air temperature. All different layers of information were classified as standard maps by expert judgment and field visits, and each category is ranked from 1 to 10 according to its degree of importance. Also, each layer is assigned an appropriate weight based on the groundwater potential using the hierarchical analysis process. The resulting map of the study area was quantitatively and qualitatively zoned into five classes: excellent, good, moderate, very low, and poor. The results obtained were compared with field electrical resistivity surveys and a high correlation was found. The results obtained from the groundwater potential map were validated by comparison with lithologic and water-level data, thus demonstrating the accuracy of the applied method.

Keywords Asadabad plain · Electrical resistivity · GIS · Groundwater potential · Iran · Remote sensing

Introduction

Groundwater is a reliable source of water in arid and semi-arid regions (Tizro 2002; Eslamian et al. 2014). However, determining suitable locations for groundwater extraction

in such regions remains an important challenge. The technological developments of geophysical methods, remote sensing (RS), and mathematical models have reinforced the accuracy of aquifer identification and delineation. Geophysical (seismic, gravity, magnetic, and geoelectric) methods can be used to reduce substantially the number and cost of test borings in selecting sites for future exploitation of groundwater. Seismic prospecting provides fairly accurate estimates of the depth to different layers and bedrock, while gravity prospecting may be used successfully in determining caverns in limestone (Tizro et al. 2010). Ground-penetrating radar produces subsurface images of high accuracy, but its applicability is limited to aquifers with a water table depth of less than 30 m (Doolittle et al. 2006; Lambot et al. 2008). Direct current electrical prospecting includes electrical profiling, which provides information about the lateral variation of resistivity; likewise, vertical electrical sounding (VES) illuminates resistivity variation with depth (Keller and Friscknecht 1966; Zohdy et al. 1974). Geoelectric methods are used to obtain information on the depth and type of material (e.g., consolidated vs. unconsolidated), bedrock conditions (e.g., fracturing), groundwater depth, salinity,

Responsible Editor: Amjad Kallel

✉ Abdollah Taheri Tizro
ttizro@basu.ac.ir

- ¹ Department of Science and Water Engineering, Faculty of Agriculture, Bu-Ali Sina University, Hamada, Iran
- ² Institute of Hydrology of the Slovak Academy of Sciences, Dúbravská cesta 9, 84104 Bratislava, Slovakia
- ³ Department of Earth and Environmental Sciences, University of Kentucky, Lexington, KY 40506-0053, USA
- ⁴ Laboratory of Engineering Geology and Hydrogeology, Department of Geology, Aristotle University of Thessaloniki, Thessaloniki, Greece
- ⁵ UNESCO Center (Cat. II) for Integrated and Multidisciplinary Water Resources Management, AUTH, Thessaloniki, Greece

pollution, and the direction and velocity of groundwater flow (Bouwer 1978; Urish 1983; White 1994; Samouëlian et al. 2003; Song et al. 2012). Tizro et al. (2010) found that aquifer transmissivity is directly related to transverse resistance in the VES method. Recent studies using geoelectric methods to determine areas of high groundwater potential have focused on data analysis (Younis et al. 2019; Mainoo et al. 2019; Rajkumar et al. 2019; Rusydy et al. 2020).

Remote sensing is a reliable tool for preparing thematic maps over large areas (Ganapuram et al. 2009). It is useful for estimating the amount of available groundwater and the management of groundwater resources, such as determining recharge areas or groundwater abstraction zones (Oikonomidis et al. 2015), especially in developing countries due to the lack of sufficient field data and hydrogeological maps. However, RS generally does not provide high accuracy in estimating the water table position (Sener et al. 2005). The integration of RS with geographic information systems (GIS) facilitates the use of all spatial data in the study area (Nagarajan and Singh 2009). Using a common database for these two methods, it is possible to draw different thematic maps. For example, Elewa and Qaddah (2011) used the RS/GIS combination to map the groundwater potential in the Sinai Peninsula (Egypt). The parameters used in this research included rainfall, groundwater recharge, lithology or infiltration rate, lineament density, land slope, drainage, and groundwater depth. However, other effective parameters, such as groundwater quality, technical and economic issues, and regional geomorphology are also important in determining areas prone to groundwater recharge/abstraction or vulnerable to pollution (Voudouris et al. 2010). Antonakos et al. (2014) suggested a fuzzy decision support system using GIS to identify the most suitable sites for drilling new boreholes for drinking water. Narany et al. (2016) proposed a GIS-based approach with water quality indices and hydrogeological factors to assess suitable zones for irrigation using groundwater.

As discussed above, the identification of the best places for groundwater exploitation and drilling wells has been a challenge for local authorities to save economic resources. In the past several decades, geoelectric methods have played an important role in determining the suitable area for water extraction with satisfactory accuracy. However, less area could be covered with this method and there are growing appeals for remote sensing methods in different parts of the world with no limitations. The application of the RS method is maturing with a wealth of well-understood methods and algorithms. We also planned to deploy this method considering several different parameters which affect the performance of delineating groundwater potential areas. However, there has been less previous evidence for the reliability of groundwater potentiality mapping with the RS method,

and previous research has examined their results only by using drilling data. Therefore, the present research made an effort to contribute to providing well-accurate VES data for selected strategic plain in the western part of Iran to validate RS results and assess better the groundwater resources. Finally, the accuracy and applicability of the two methods have been evaluated and compared with large sets of drilling data.

Location and hydrogeological conditions

The Asadabad plain is part of the Karkheh basin with a location of 47°52' to 48°15' E and 34°37' to 34°56' N in the west of Hamadan province in Iran. The Asadabad catchment area is 582 km². The annual temperature range is -9 to 35 °C, and the average annual rainfall is about 340 mm. The catchment is under the influence of Mediterranean frontal systems, and most precipitation falls from February to March. Based on the De Martonne (1923) aridity index, the climate is semi-arid. Significant crops in the region include irrigated and rain-fed wheat, barley, potatoes, and tomatoes.

The Asadabad plain is covered by Quaternary alluvium. The lithology of the plain consists of four main parts, which include (1) Triassic-Jurassic slates and phyllites in the east; (2) sedimentary rocks in the north, south, and west; (3) Jurassic-Cretaceous formations in the west; and (4) Cretaceous carbonates in the south and west (Iran Water Resources Management Company 2004). The area lies within the Sanandaj-Sirjan tectonic zone and is surrounded by mountains with maximum elevations > 3000 m above mean sea level (amsl). Igneous (both intrusive and extrusive), metamorphic, and sedimentary rocks are exposed in the area (Huber 1953). The area has been mapped at the 1:250,000 scale by the Geological Survey of Iran and its geological setting is described by Braud (1970) and Boulourchi (1979). According to reports in the literature, schist and limestone are the dominant compositions in most of the depth profiles from the surface to bottom rock in the Asadabad plain. The larger sediments are located at the plain margin while fine-grained particles (mostly clay and silt) have formed the sediment texture of the plain center (Fig. 1), having high permeability due to the essence of fine-grained parts. The main aquifer systems have been formed within alluvial sediments. They are divided into two aquifers, the unconfined one (marginal area) and the semi-confined one (central part). The thickness of alluvial sediment varies from 50 m on the margin of the plain to more than 300 m in the center (Bagheri 2017).

The largest river in the region, which collects almost all of the plain runoff, is located in the center of the Asadabad plain and is 50-km long. Shahab and Darband are

the most important rivers in the region. The general slope of the catchment is from northeast to southwest (Fig. 1). The drainage patterns are dendritic in character. In some seasons, the rivers are with less runoff, and in the dry period, they become non-entities with no water flow. The average depth of water in the Asadabad plain is about 30 m below the surface. It should be noted that the average water drop in the last 10 years was predicted about 17 m due to the increase in the number of unauthorized deep wells in the plain.

Materials and methods

Data used in this research include geological maps of the area (scale 1:100,000); a Landsat-8/ETM satellite map; digital elevation models (DEMs) of ASTER and OLI satellites with a horizontal and vertical spatial accuracy of 15 m; and meteorological and groundwater-level measurements. For this study, monthly rainfall and air temperature data from 2006 to 2016 were obtained from the four meteorological monitoring sites operated by the Meteorological Organization of Hamadan Province. Water levels were measured for 23 piezometers (Fig. 1) at almost the same time in the year 2016. The geological maps were prepared and entered into ArcGIS 10.3 software to be localized with the UTM/WGS84 coordinate system. The data strips in the satellite imagery were then retrieved by ENVI 5.1 software for a similar location as the geological layers by changing the image size and reducing the error. The thematic maps, including rainfall, lithology, lineament density, land slope, drainage network, and water table depth, were prepared. Finally, a weighted probabilistic-spatial method was developed to prepare the groundwater potential map in the area at the approach described in Fig. 2. The obtained map includes five different classes to show the existence of groundwater resources (excellent, good, moderate, very low, and poor).

The analytic hierarchy process (AHP) developed by Saaty (1980) was used to weight and map the groundwater potential, as has been done elsewhere (Malczewski 1999; Pourghasemi et al. 2012; Oikonomidis et al. 2015). In this method, the factors affecting the groundwater potential are weighted based on their effectiveness. The effective parameters are paired and after determining their importance to each other, arithmetic values between 1 and 9 are assigned to each of them according to their degree of importance in this comparison (Table 1). The number 9 indicates the highest importance and impact on a potential acquisition, whereas the number 1 indicates that both parameters are equally important. After the completion of Table 1, the arithmetic mean method has been applied to its results (Table 2). The overall consistency ratio obtained for these judgments (0.075) indicated no need

to recalculate the procedure for weights of the effective parameters. Finally, the potential groundwater resources map is prepared by combining the weighted layers following Equation 1.

$$M = \sum_{i=1}^n W_i X_i \quad (1)$$

The weighted average method is used to calculate M as the value of each pixel of the final map. The value of weight (W_i) applied to each parameter (X_i) affects the determination of areas prone to groundwater. It should be noted that the quality parameters were classified by the map guide grading method with unequal intervals and based on the importance of each degree in ArcGIS software. This method has been used by some researchers in hydrological studies for the determination of degrees of vulnerability in an area (Huan et al. 2012; Kazakis and Voudouris 2015).

Vertical electrical soundings were conducted with the Schlumberger configuration because of its various advantages (Bhattacharya and Patra 1968; Keller and Friscknecht 1966; Zohdy 1989; Song et al. 2007), particularly the interpretation techniques available. The maximum current electrode was kept between 400 and 500 m. The field apparent resistivity data for different values of $AB/2$ (AB , the distance of transmitter electrodes) were processed for 73 vertical electrical soundings (see Fig. 17 for VES points). In this study, an attempt was made to determine ranges of apparent resistivity for different lithologic layers. Resistivity varies from 35 to 100 ohm-m for sandy horizons, for predominantly clayey zones 3 to 25, and from 150 to 400 ohm-m for lithified units (Nejad et al. 2011; Tizro et al. 2012). Low resistivity values for rock formations imply their friable and weathered nature. IPI2win software was used to interpret the data obtained from vertical electrical sounding (Bobachev 2002).

Results

In this study, eleven factors have been used to identify the groundwater potential areas, including rainfall, lithology, drainage density, lineament density, land use, topography, slope, slope aspect, distance from waterways (streams), distance from lineaments, and air temperature. Thematic maps have been analyzed separately and used to calculate the final groundwater potential map in the area. The applied weights in previous studies have been considered in the study of groundwater status in the region (Tizro et al. 2010).

Rainfall and topography

Rainfall is one of the most important factors affecting the potential of groundwater and weights 0.233 (Table 2).

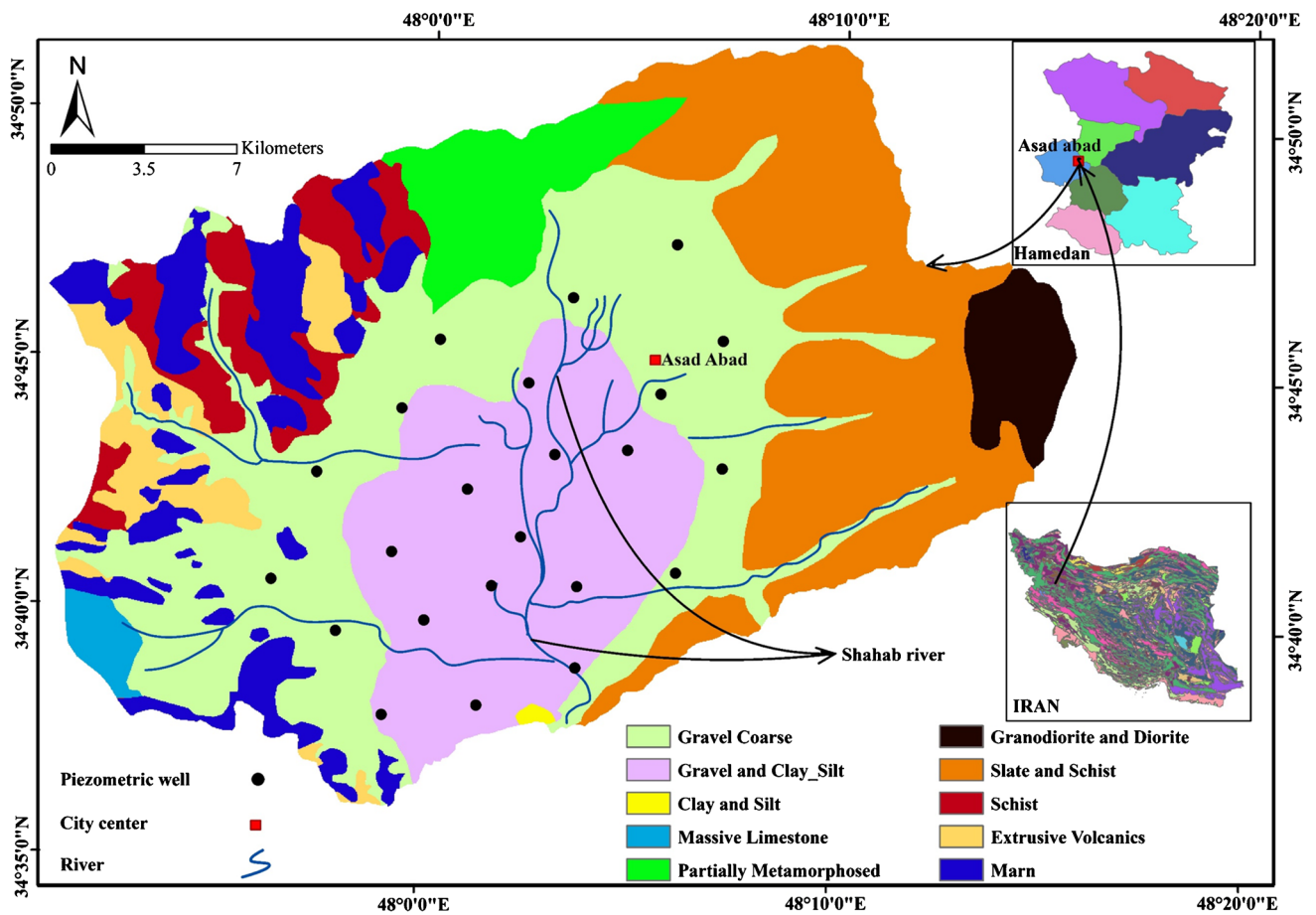
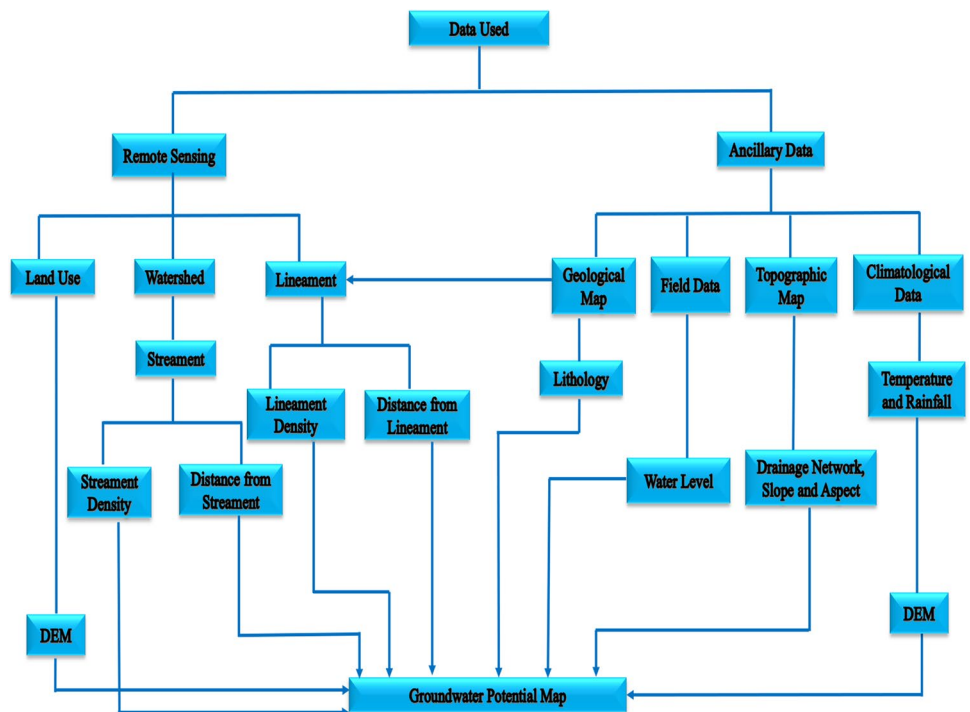


Fig. 1 Map showing the location and geology of the study area with piezometric wells

Fig. 2 Flow chart of operations performed



Isohyetal maps were interrogated by kriging using the interpolation tool in ArcMap. As shown in Figure 3, rainfall ranges from 325.26 to 449.15 mm, with the lowest values in the center of the plain and the highest in the west. Elevation ranges from 1433 m amsl at the outlet of the basin in the south to 2782 m amsl in the east (Fig. 4) and rainfall increases with altitude. The weight of topography has been calculated as 0.046 (Table 2).

Lithology

Lithology (weight 0.233, Table 2) is related to permeability and affects the storage capacity of aquifers via matrix porosity and fractures. For most of the plain, the surficial lithology consists of gravel interspersed with clay and silt (in the central part) or coarse gravel (adjoining the central part), which have relatively high porosity (Fig. 5). In the surrounding upland areas, igneous and metamorphic rocks and marls, which tend to be less permeable, promote runoff into stream valleys, where infiltration will be more favorable.

Land use

The presence of vegetation (Fig. 6), which was inferred from Landsat images, reduces the surface flow velocity and promotes infiltration. The location of horticulture and dense pastures, particularly in the central plain, has created very favorable conditions for the infiltration of surface water, although vegetation may also limit groundwater recharge because of plant water uptake. The calculated weight for land use is 0.116 (Table 2).

Lineament density

Lineaments tend to correspond with regional-scale joint and fracture sets, which promote infiltration and can create secondary porosity in aquifers. Landsat 8 images were processed in ENVI software, and then the lineament density was calculated using ArcMap and classified into five groups, as shown in Figure 7. The computational weight for lineament density is 0.078 (Table 2). The highest lineament densities coincide with exposures of crystalline rocks in the northern and eastern parts of the region.

Drainage density

Drainage density is the ratio of the total length of all waterways and rivers in a drainage basin to the total area of the basin and indicates how water is discharged from the plain area. As drainage density decreases, the rate of infiltration increases, which occurs along losing stream reaches in the center of the Asadabad plain. Thereby, the groundwater potential increases (Saraf and Choudhury 1998). Drainage

Table 1 Pairwise comparison of the preparatory factors that affect groundwater potential

	Lithology	Rainfall	Land use	Lineament density	Drainage density	Slope	Topography	Distance from streams	Distance from lineament	Slope aspect	Temperature
Lithology	1	1	2	3	3	5	5	5	5	7	9
Rainfall		1	2	3	3	5	5	5	5	7	9
Land use			1	3	3	5	5	5	5	7	9
Lineament density				1	1	3	3	3	3	5	7
Drainage density					1	3	3	3	3	5	7
Slope						1	1	1	1	5	7
Topography							1	1	1	5	7
Distance from streams								1	1	5	7
Distance from lineament									1	5	7
Slope										1	5
Temperature											1

Table 2 Calculation of factor weights (in combination with Table 1)

Lithology	Rainfall	Land use	Lineament density	Drainage density	Slope	Topography	Distance from stream	Slope aspect	Temperature
0.233	0.233	0.116	0.078	0.078	0.068	0.046	0.045	0.033	0.026

density has been calculated by ArcMap and classified into five groups with different amplitudes (Fig. 8). The calculated weight for the drainage density drainage layer is 0.078 (Table 2).

Slope and slope aspect

Another factor that determines the hydraulic gradient and the direction of groundwater movement is the surface slope. Generally, runoff is enhanced in steep areas and infiltration is promoted in flatter areas (Döll et al. 2002). Using the DEM, the slope and slope aspect were determined, with weights of 0.068 and 0.033, respectively (Table 2). The slope is generally 1–10° in the center and margin of the plain (Fig. 9), and the slope decreases southward (Fig. 10). The slope direction has the highest weight in the southern

regions and the lowest weight in the north due to the angle of solar radiation.

Distance from streams

The type of drainage network is controlled by tectonic structures, lithology, and topography and is dendritic in this region. Areas within 70 m of streams have the highest coefficient (Fig. 11) and the calculated weight for distance from streams is 0.045 (Table 2).

Distance from lineaments

As noted above, infiltration and secondary porosity can increase with lineament density. Similarly, reduced distance from a lineament is related to increased groundwater

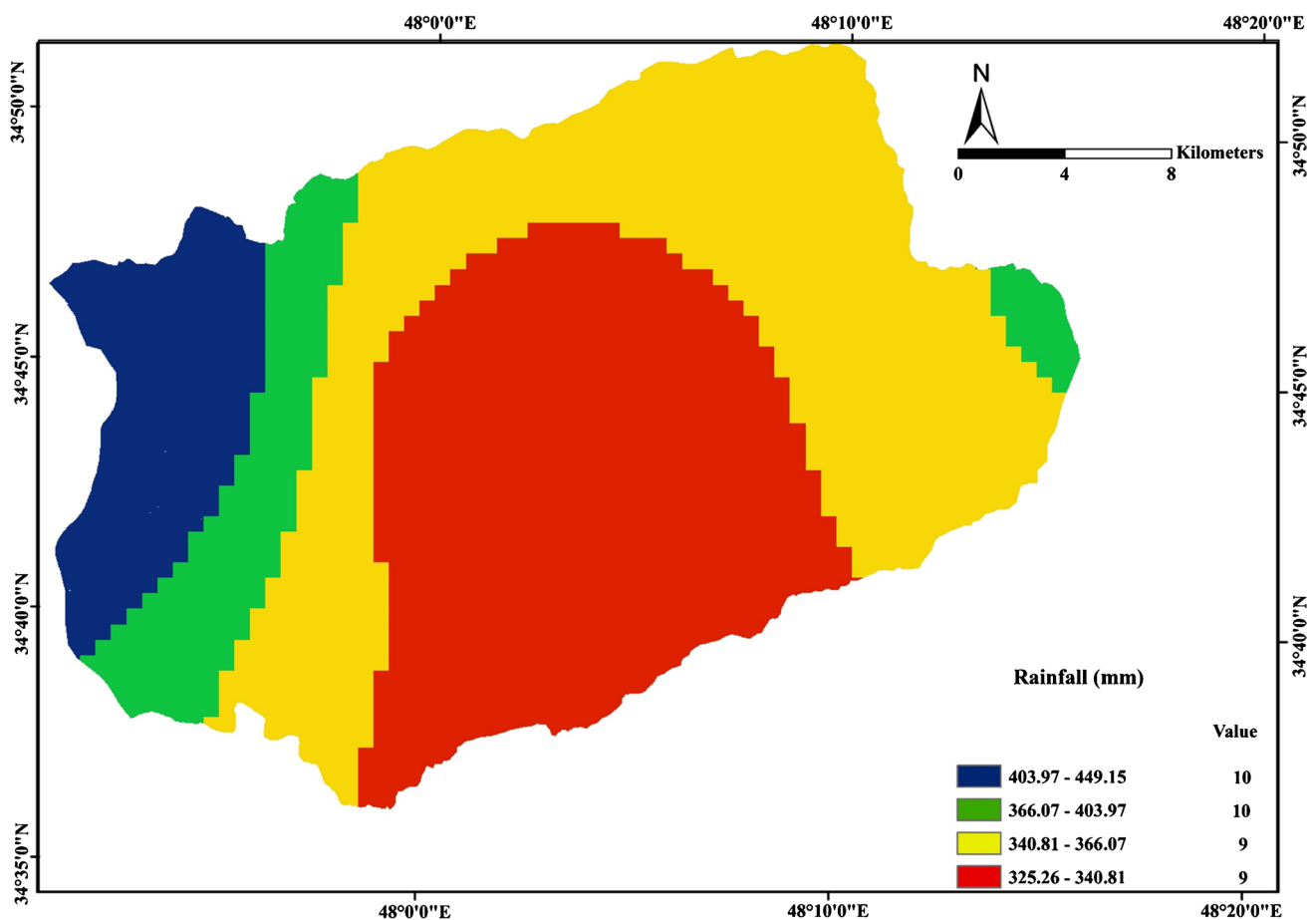


Fig. 3 Rainfall map of the study area, divided into four classes valued with two weights

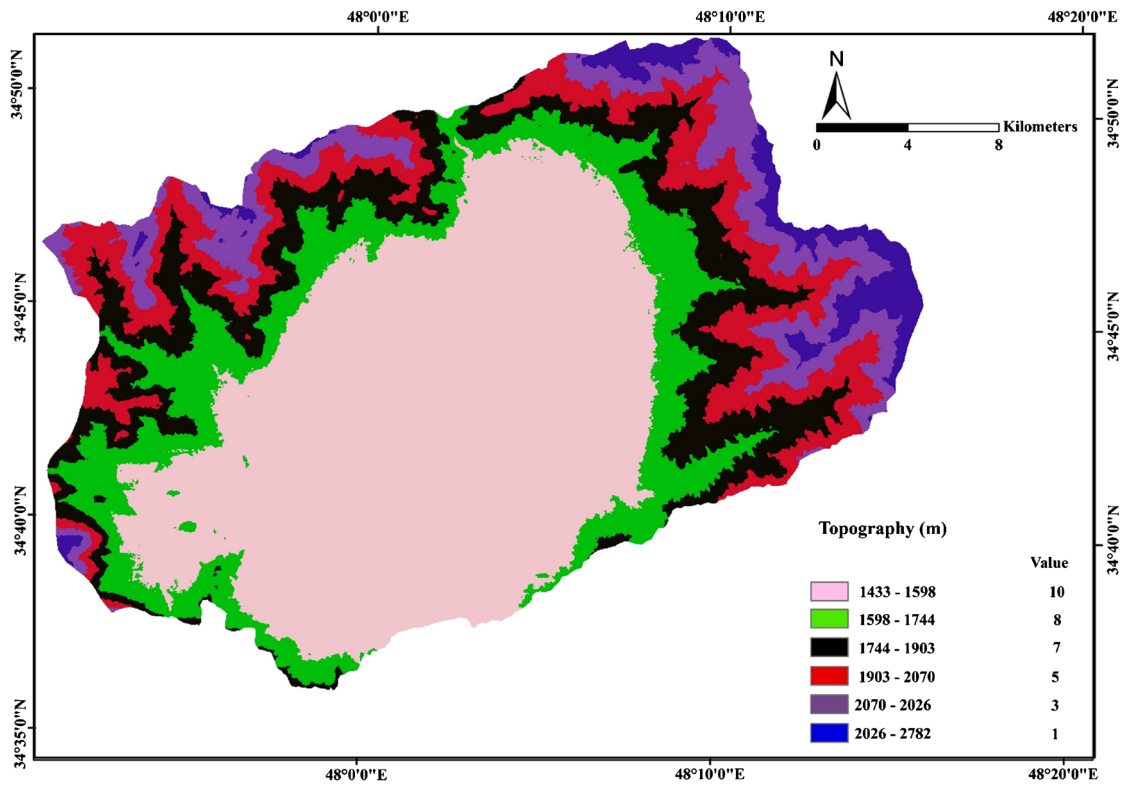


Fig. 4 Topographic map of the study area.

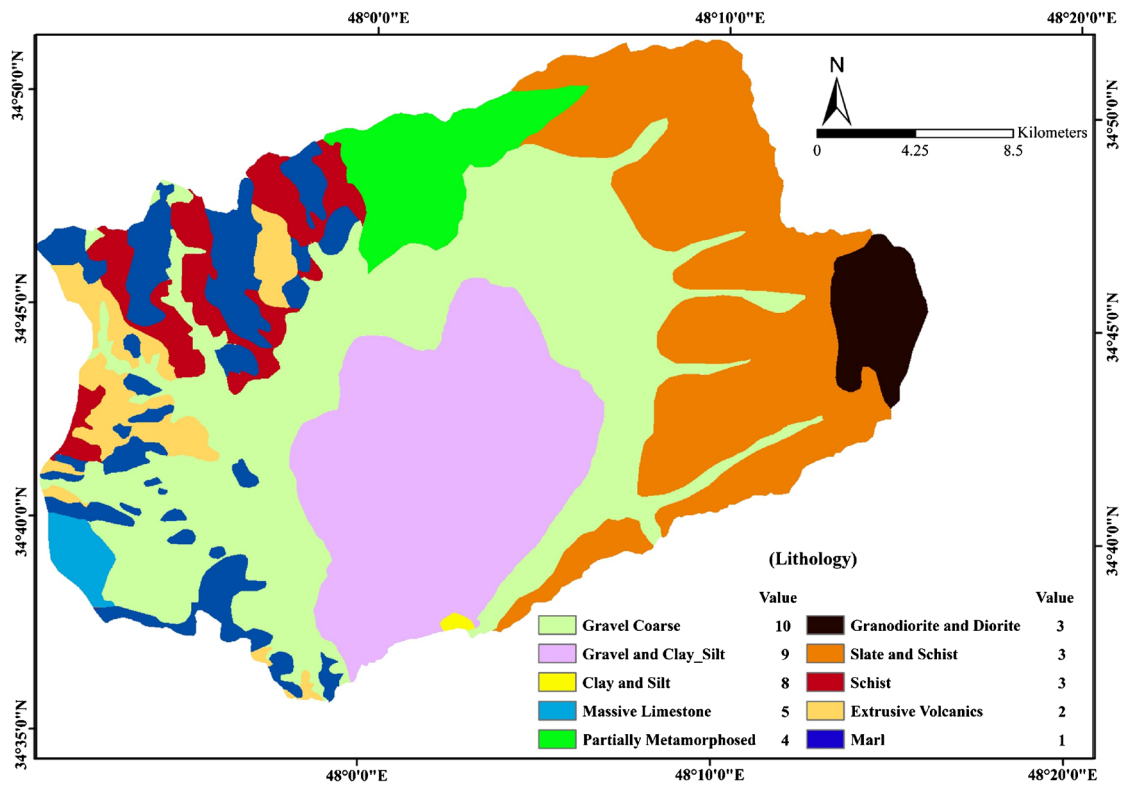


Fig. 5 Lithologic map of the study area divided into classes with values from 1 to 10

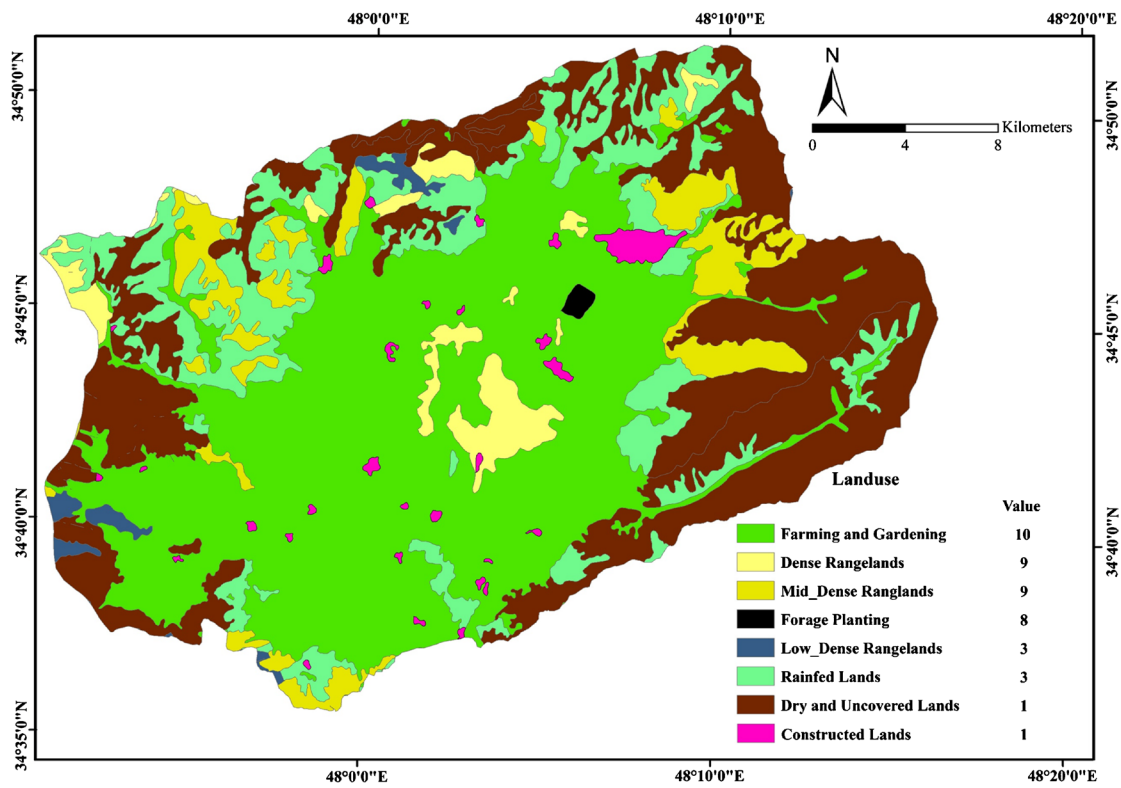


Fig. 6 Map showing land use classes of the study area with corresponding values

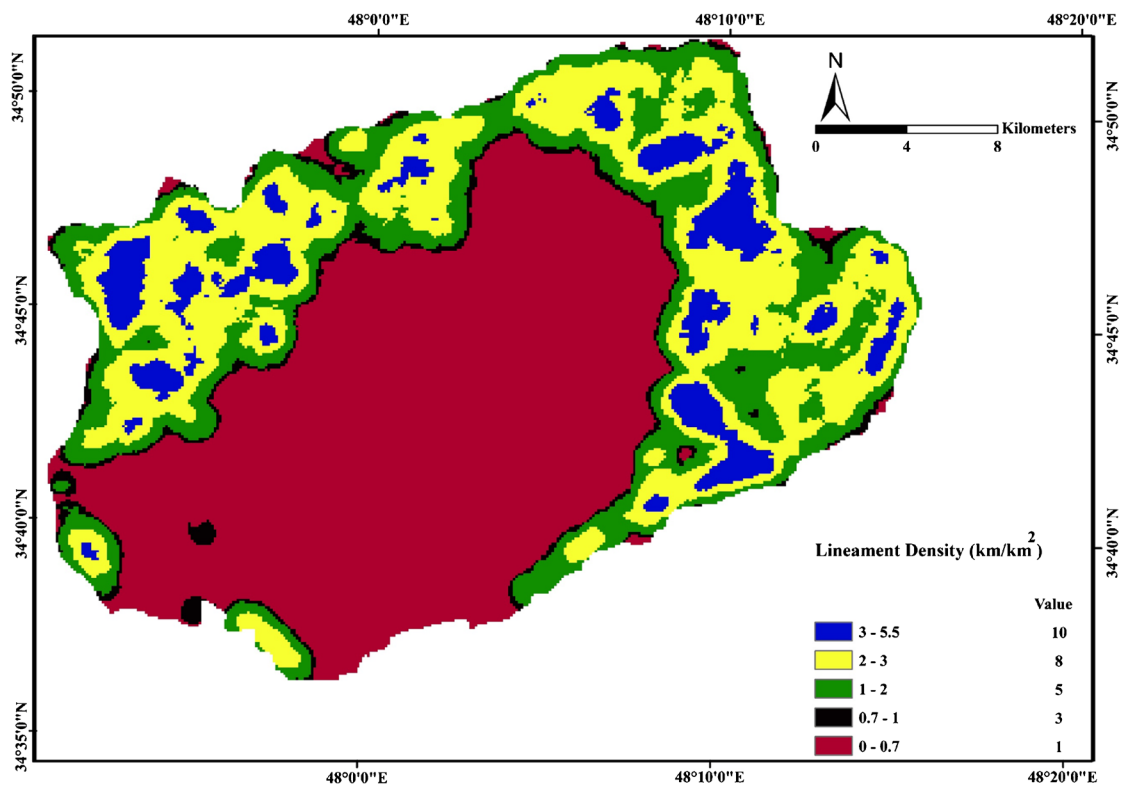


Fig. 7 Lineament density map of the study area, divided into five classes

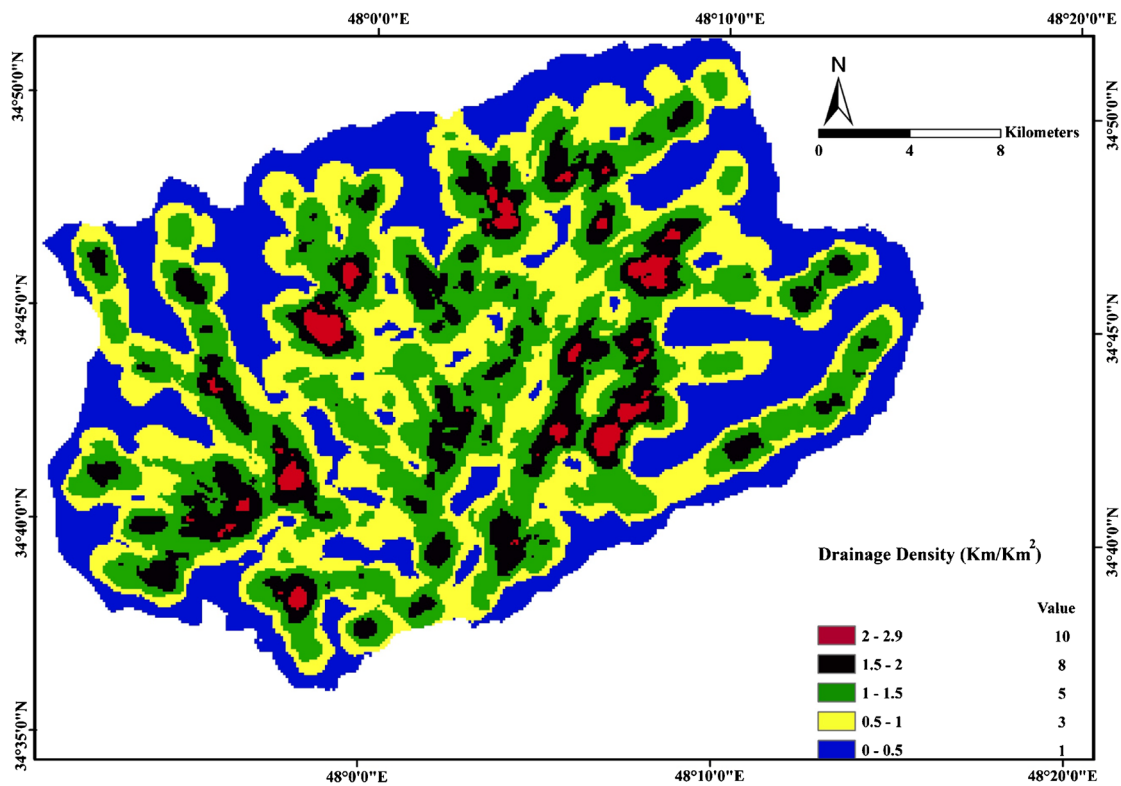


Fig. 8 Drainage density map of the study area, divided into five classes

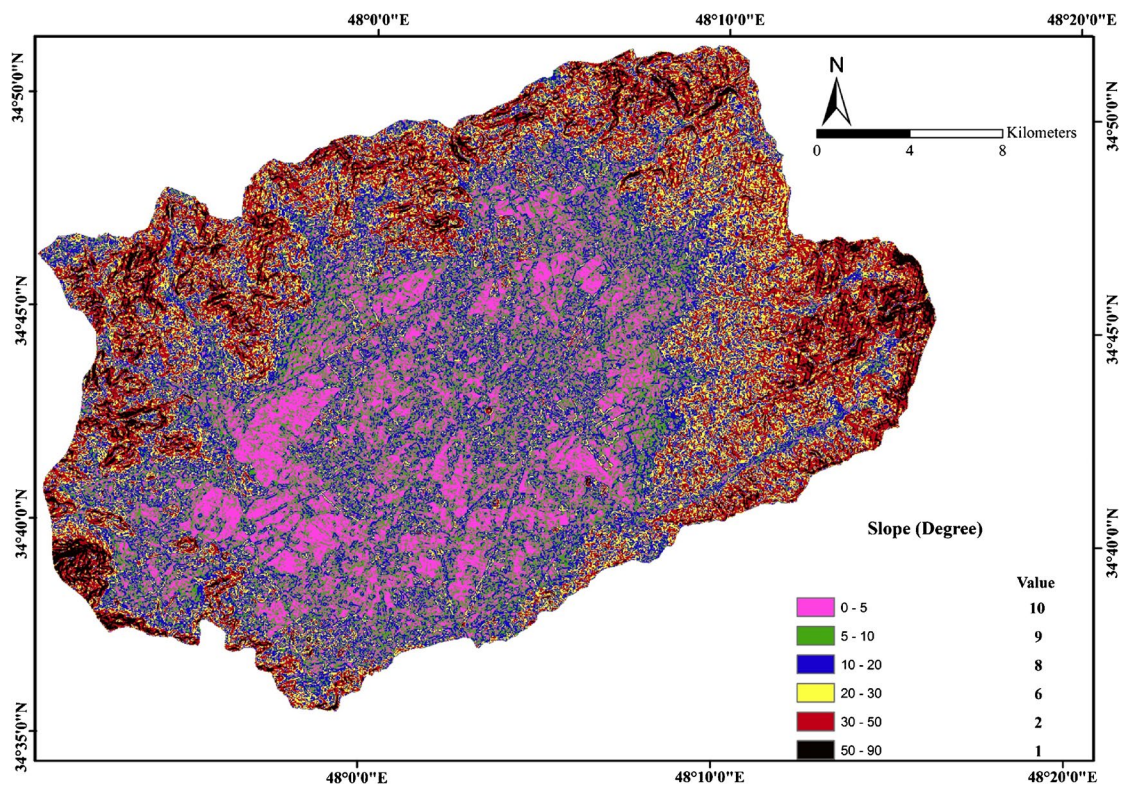


Fig. 9 Slope map of the study area with classes from 0 to 90°

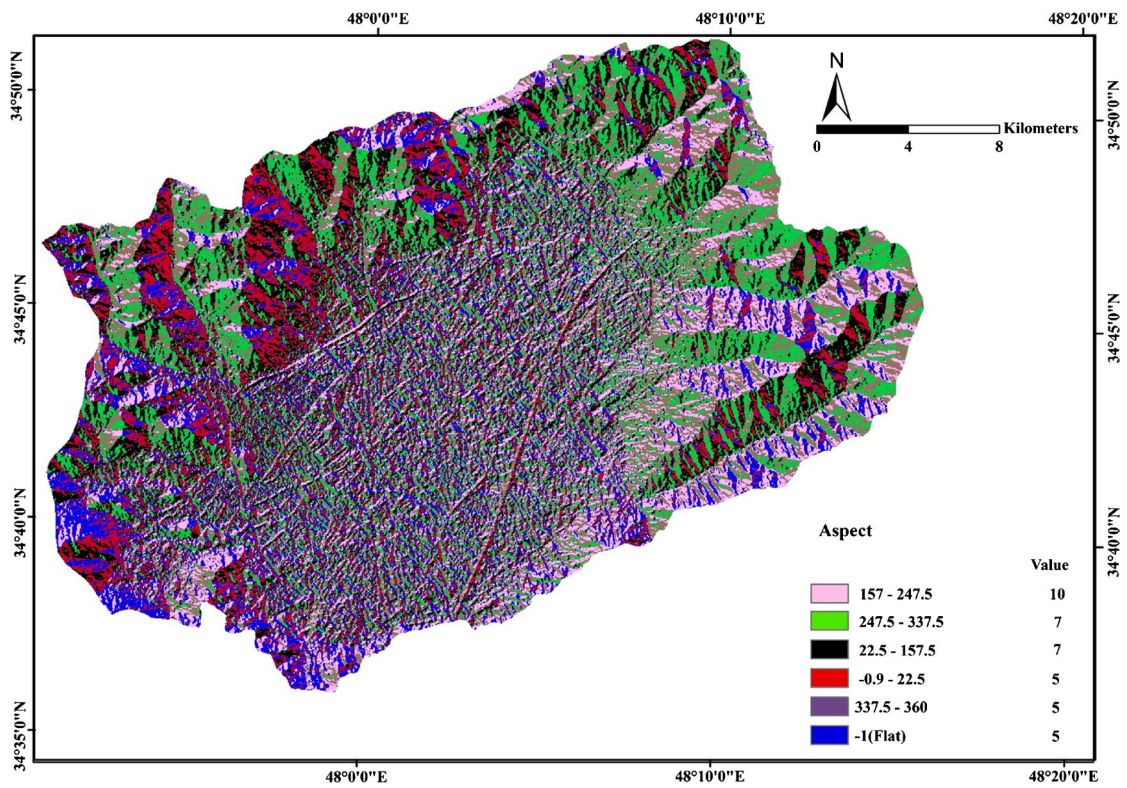


Fig. 10 Aspect slope map of the study area in five classes

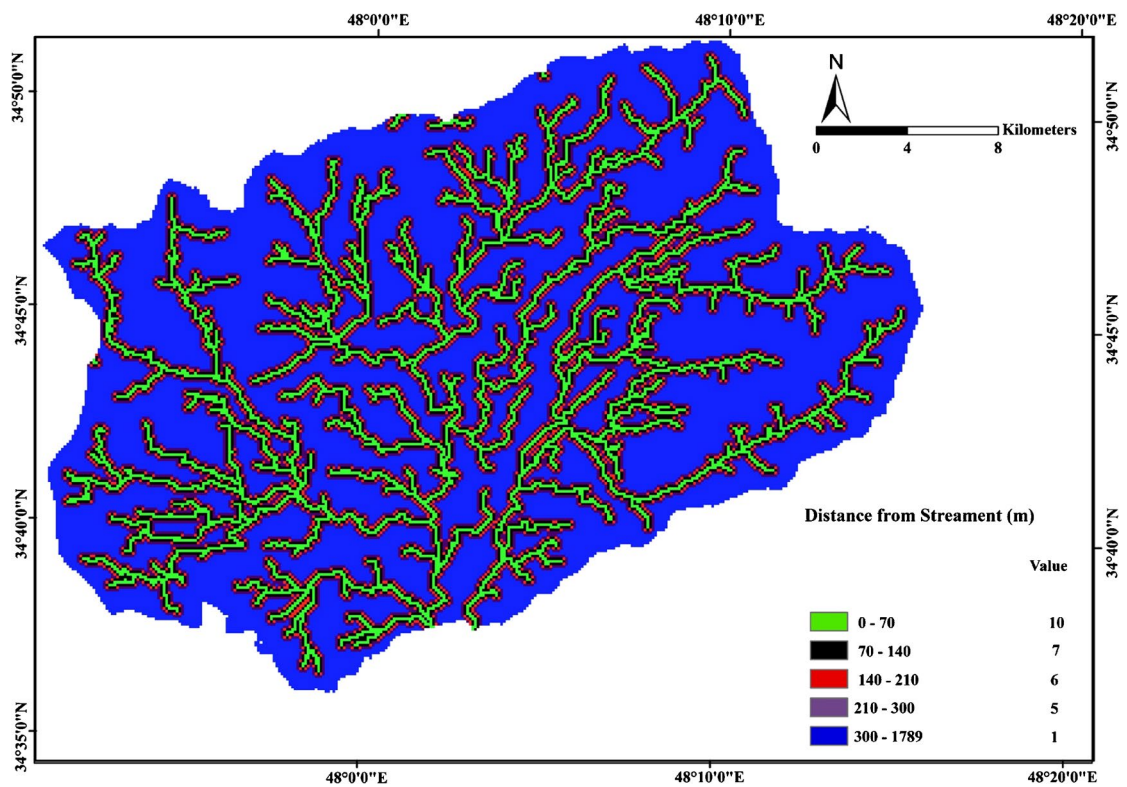


Fig. 11 Map showing the distance from streams in the study area

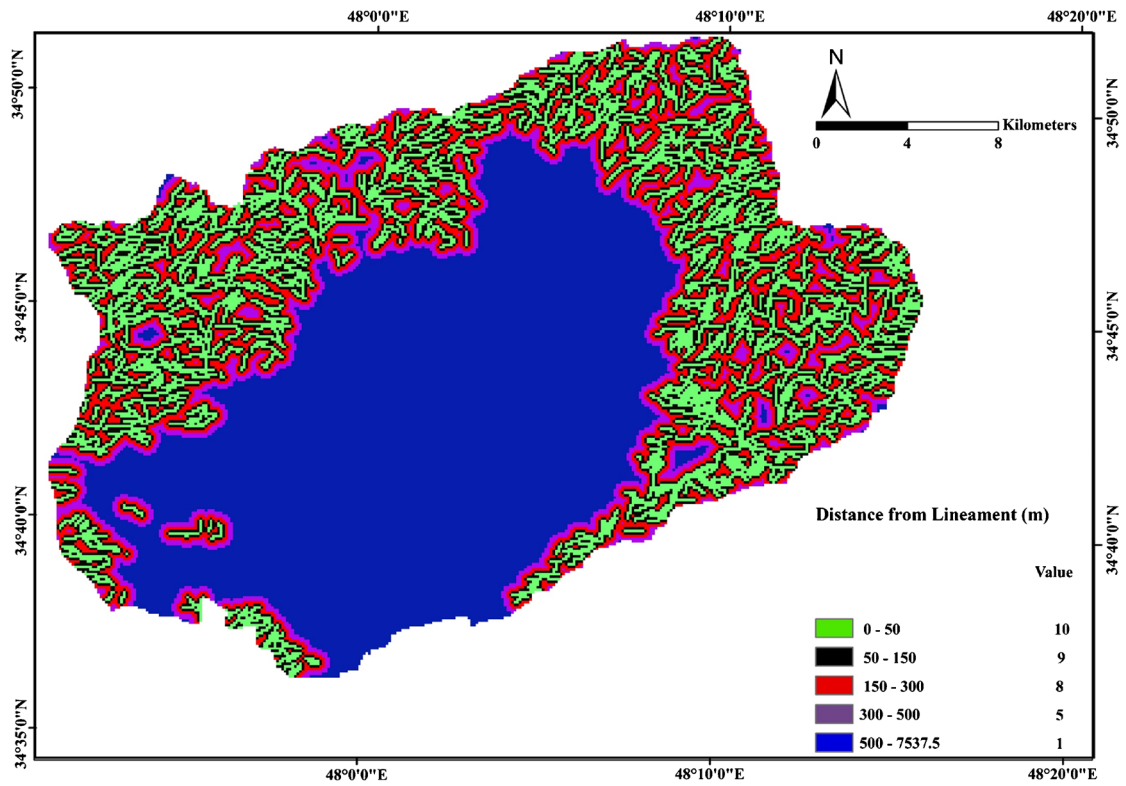


Fig. 12 Map showing the distance from lineaments in the study area

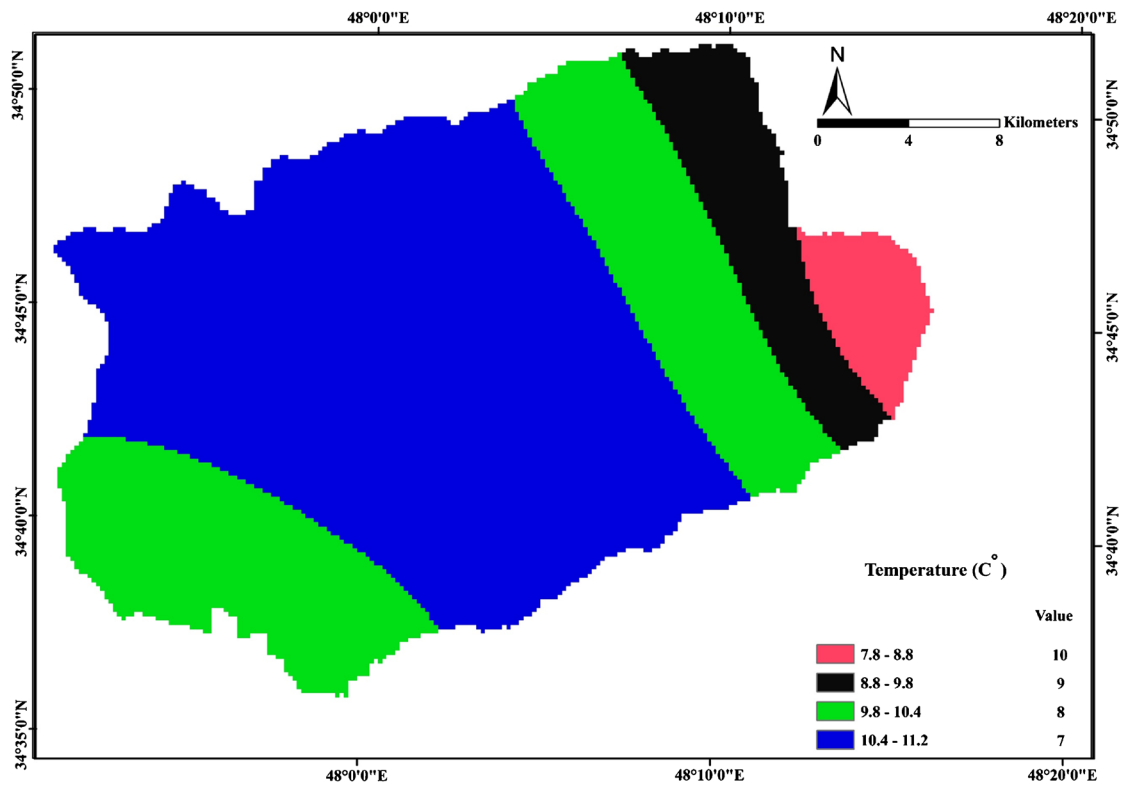


Fig. 13 Distribution of air temperature in the study area

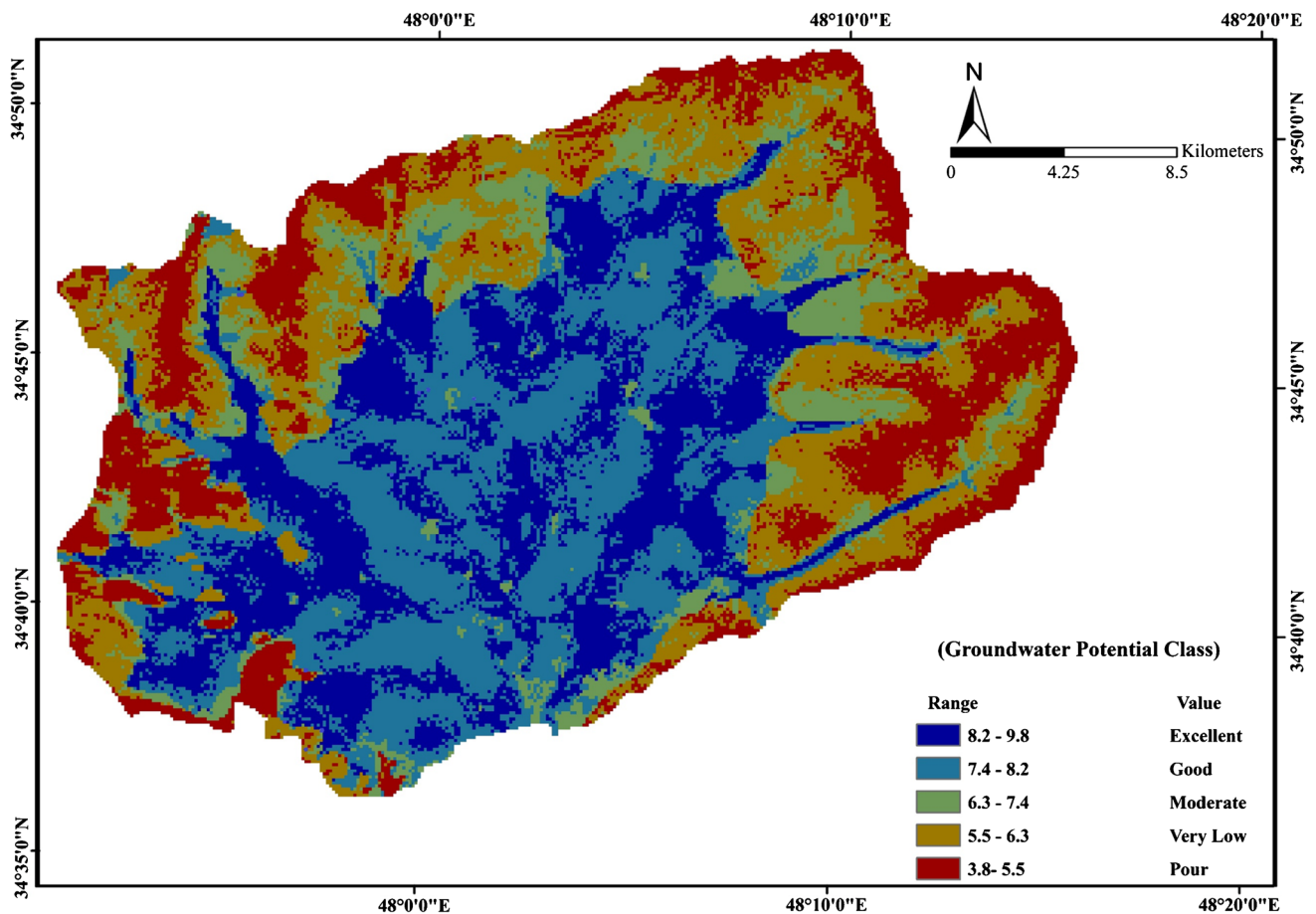


Fig. 14 Groundwater potential map of Asadabad plain

potential. Distance to lineaments is lowest (< 50 m) in upland areas of the basin and greatest in the basin center (Fig. 12). The calculated weight for this factor is 0.044 (Table 2).

Air temperature

Infiltration is reduced as evaporation increases with temperature. The temperature map, which was created by kriging in ArcMap, indicates values are highest in the central part of the basin and lowest in the east (Fig. 13). The weight of this factor is 0.026 (Table 2).

Final map and discussion

The weight of each raster layer was applied to calculate the groundwater potential for each pixel (Elewa and Qaddah 2011). The zoning raster map was divided into five classes using the natural failure method with unequal distance method in grading (Fig. 14). This classification method reduces the variance within classes and increases the variance between classes. The intervals are defined as

Table 3 Resistivity ranges for different lithological units

Resistivity (ohm-m)	Lithologic units
10–300	Surface alluvial deposits
15–200	Alluvial deposits probably containing groundwater
5–20	Zone with high clay content and schist
150–220	Weathered schist
170–200	Slate, schist, and weathered schist
20–30	Limestone
200–300	Massive limestone
80–200	Conglomerate and sandstone
170–450	Schist
40–200	Slate and schist
400–1200	Extrusive volcanic rocks
20–40	Marl
100–250	Limestone with marl
150–400	Marl with schist and limestone
300–1500	Marble with sandstone
500–700	Granodiorite and diorite

Fig. 15 A selected field sounding curve of profile F

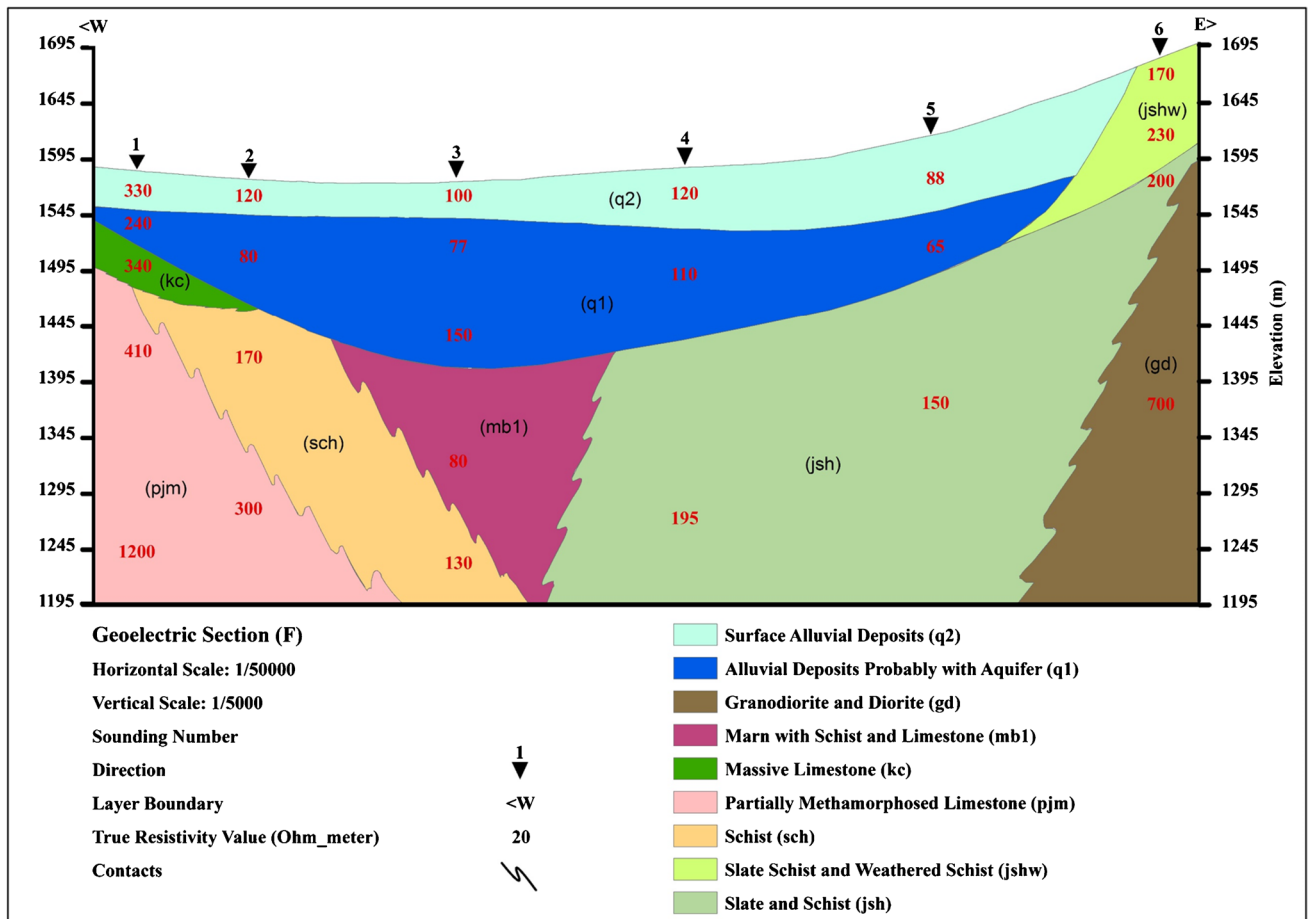
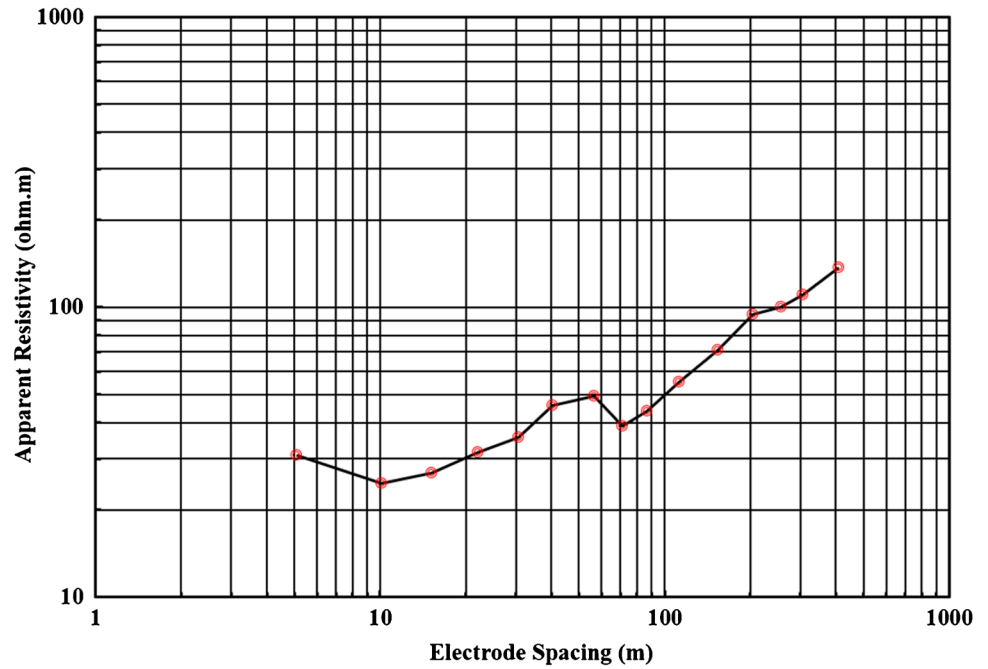


Fig. 16 Geoelectric cross-section along with line F

poor (3.875–5.535%), very low (5.535–6.352%), moderate (6.352–7.403%), good (7.403–8.244%), and excellent (8.244–9.832%). The highest values generally occur in the central part of the plain and along stream channels, whereas the lowest values tend to occur around the margins of the plain. Higher potential access in the south-central part of the plain is attributed to the higher potential recharge in this area due to hydrogeological and morphological characteristics such as gravel material and low slopes. Collectively, suitable groundwater potential zones locate mostly in midland and lowland regions due to higher infiltration potential; while low groundwater potential zones are usually demarcated in the highlands due to higher runoff on steep slopes (Arulbalaji et al. 2019).

Groundwater potential maps have been widely used to select sites for well drilling and regional management of groundwater (Chen et al. 2019). These maps are commonly developed using GIS (Al-Abadi et al. 2016). Remote sensing techniques have been also used for fault detection and morphological analysis (Machiwal et al. 2011; Abuzied et al. 2020) with appropriate accuracy, more than 80% (Jhariya et al. 2021). Additionally, AHP has been used to

overcome the subjectivity of weight delineation of model parameters (Rahmati et al. 2015; Kazakis 2018). Ganapuram et al. (2009) deployed the combinations of RS/GIS to depict groundwater potential zones in the Musi basin in India. The results showed that potential zones include floodplains, alluvial plains, and deep pediplain due to the composition of alluvium and weathered material forming the basin layers. The place was covered with piedmont plain, denudational hills, and the linear ridge was not recommended for groundwater exploitation. A similar pattern of results was obtained in the present study showing dense pastures located at the south-central part of the plain with favorable groundwater levels. It is worth mentioning that the presence of gravel in the south-central part of the Asadabad plain is a big advantage for having higher infiltrations and lower depth to the water table. The present findings are directly in line with previous findings in Wadi El Laqeita located in the central-eastern desert of Egypt by Abdalla (2012). He pointed out that the Quaternary deposits and fractured Precambrian were the best groundwater prospective zones similar to the Quaternary alluvium coverage in Asadabad plain.

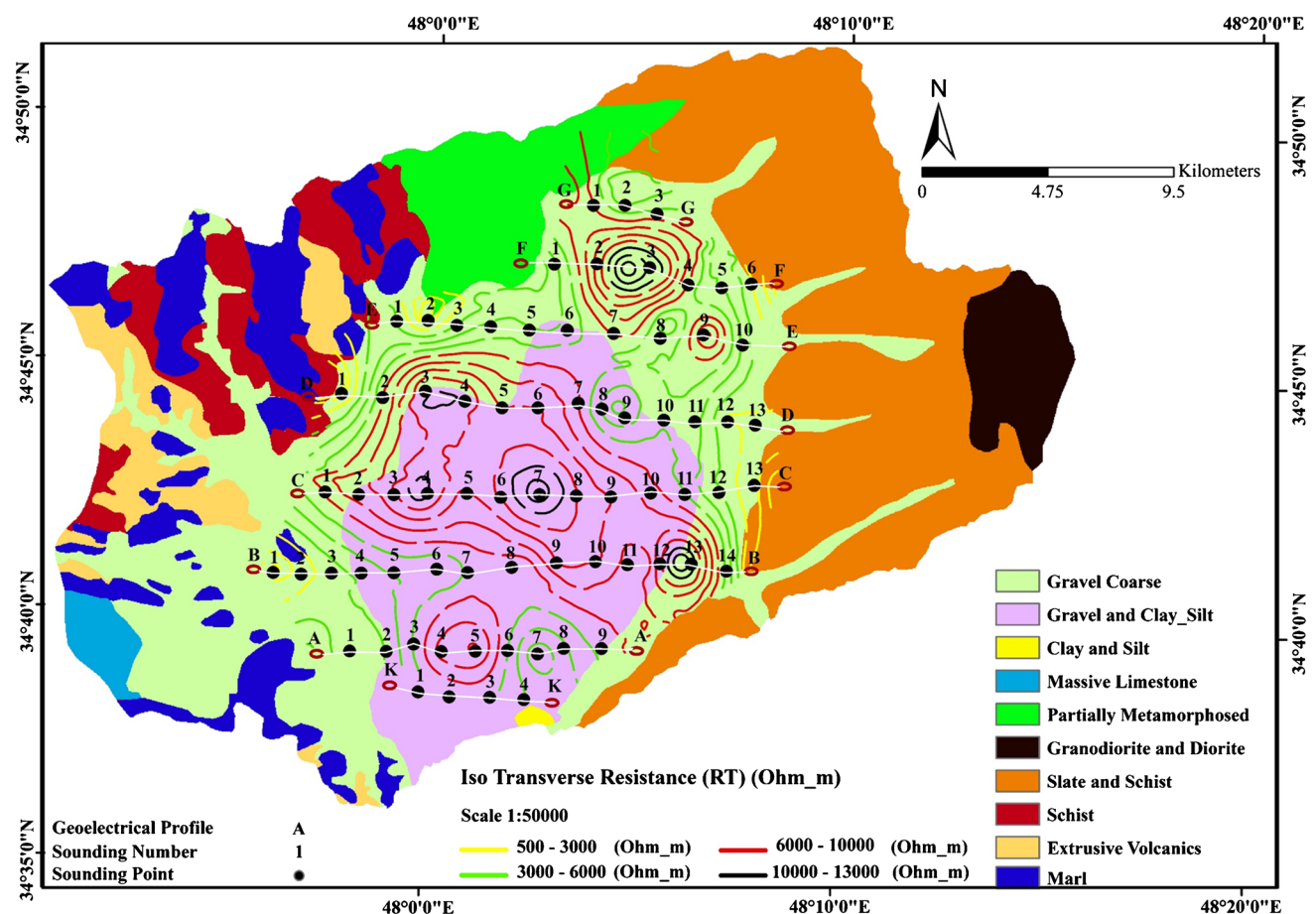


Fig. 17 Transverse resistance map

One of the recent new methods in similar studies is the adaptive neuro-fuzzy inference systems (ANFIS) algorithm which needs large data sets for building models and validation (Chen et al. 2019). The critical issue is the reliability of the initial data, including hydrogeological, hydrological, and geomorphological information. Further statistical evaluation of results has demanded the model validation to increase the resolution of the final map. Commonly used methods include evidential belief function (Park et al. 2014), weights of evidence (Al-Abadi and Shahid 2015), and the frequency ratio (Naghibi et al. 2017). Moreover, the final maps should be verified by field measurements, as was done in this study, and the initial results should be updated.

Validation

Geoelectric results

Using 73 VESs along eight profile lines (Fig. 17), the range of electrical resistivity of lithologic units was investigated. In theory, the location of the water table can be determined

by VES (Liu et al. 2007), but in practice, factors such as salinity, plant roots, texture, and temperature affect the resistivity of soil (Sudduth et al. 2003; Mainoo et al. 2019). Based on geological information, the range of variation in the resistivity of the lithologic units in the Asadabad plain is presented in Table 3. A selected curve related to the VES performed on profile F is shown in Figure 15.

Profile F, which is composed of six sounding stations, is shown in Figure 16. In this section, the surface layer composed of dry alluvial sediments (q2) covers the entire cross-section. The thickness of this layer ranges from ~ 20 m below sites F1, F2, and F3 to ~ 55 m below site F5. Beneath the surface layer, alluvial sediment that may comprise an aquifer (q1) occurs along the entire section except at site F6. The bedrock below this weathered layer is composed of granodiorite and diorite. A layer of massive limestone at site F1 lies beneath the layer of alluvial sediment (q1). At site F3, a sudden decrease of apparent resistivity appears at a depth of 180 m, suggesting solution cavities in limestone.

Transverse resistance is the product of the thickness of the aquifer layer (in meters) multiplied by its resistivity

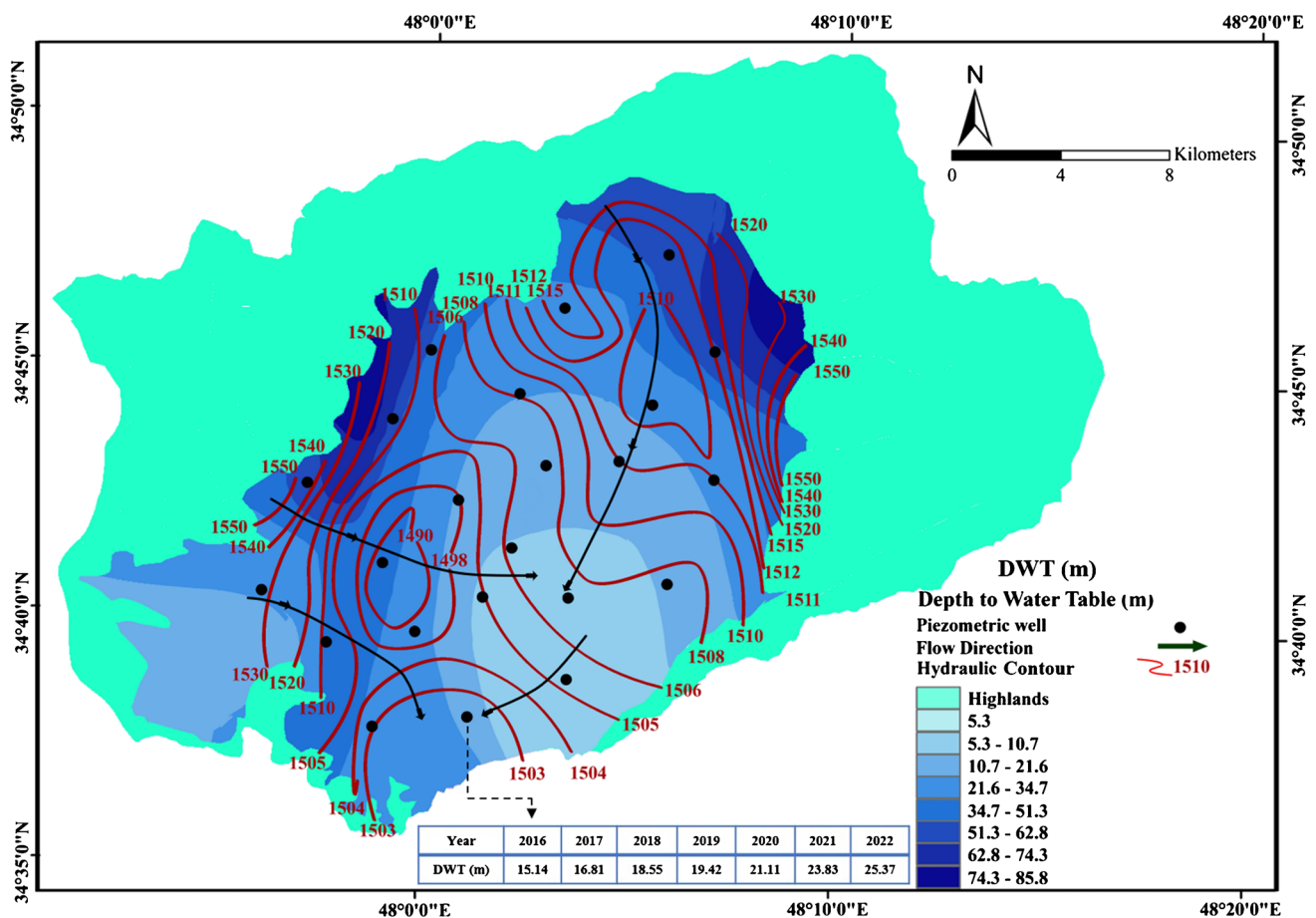


Fig. 18 Map showing the depth of groundwater in the study area with the tabulated variations of DWT in the period of 2016–2022 for the southernmost piezometric well

(ohm-m), which is expressed in terms of ohm-m². Values of transverse resistance increase from the periphery to the center of the plain (Fig. 17), with the highest values observed around sites B11, C4, C7, D4, and F3. In general, a strong connection was found between resistivity boundary and lithology variations.

Observation wells results

The depth of the groundwater below the Asadabad plain varies from 5.3 to 85.5 m (Fig. 18). It is worth reminding that the water level data were obtained in 2016 and the water table has dramatically fallen to date. For instance, the annual average depth of groundwater for a piezometric well located in the southern part of the Asadabad plain was tabulated from 2016 to 2022 (Fig. 18). The water level drop was more than 10 m for this period due to mismanagement of groundwater resources in such a strategic plain.

The direction of groundwater flow is from highland's regions in the northeast and northwest of the plain to its center and southern regions of the plain. It also can be inferred more directly by hydraulic head contours of an unconfined

(surficial) aquifer (Fig. 18). In the southern parts of the plain, the depth to groundwater is very low due to the low hydraulic conductivity and possibly the low water withdrawals.

A comparison of Fig. 14 with Fig. 18 shows that mapped areas of good to excellent groundwater potential generally coincide with shallow groundwater in the Asadabad plain, although depth to groundwater is greatest in areas of excellent potential in the west- and east-central parts of the study area. However, Fig. 14 also suggests high groundwater potential along stream valleys in upland areas which has not been monitored by piezometers in these areas; thus, the slight difference indicates a lack of data on the high land areas. In addition, the comparison of Figs. 17 and 18 shows the groundwater potential in the center of the plain increases with transverse resistance. Aquifer transmissivity decreases from the center to the edge of the Asadabad plain (Fig. 19). The aquifer transmissivity parameters were computed by a step drawdown test (Bagheri 2017). The outputs are well confirmed with previous studies attempted by the Hamadan Regional Water Organization in 2013 (Bagheri 2017).

As a check on the inferences drawn from the transverse resistance map, lithologic information of exploratory wells

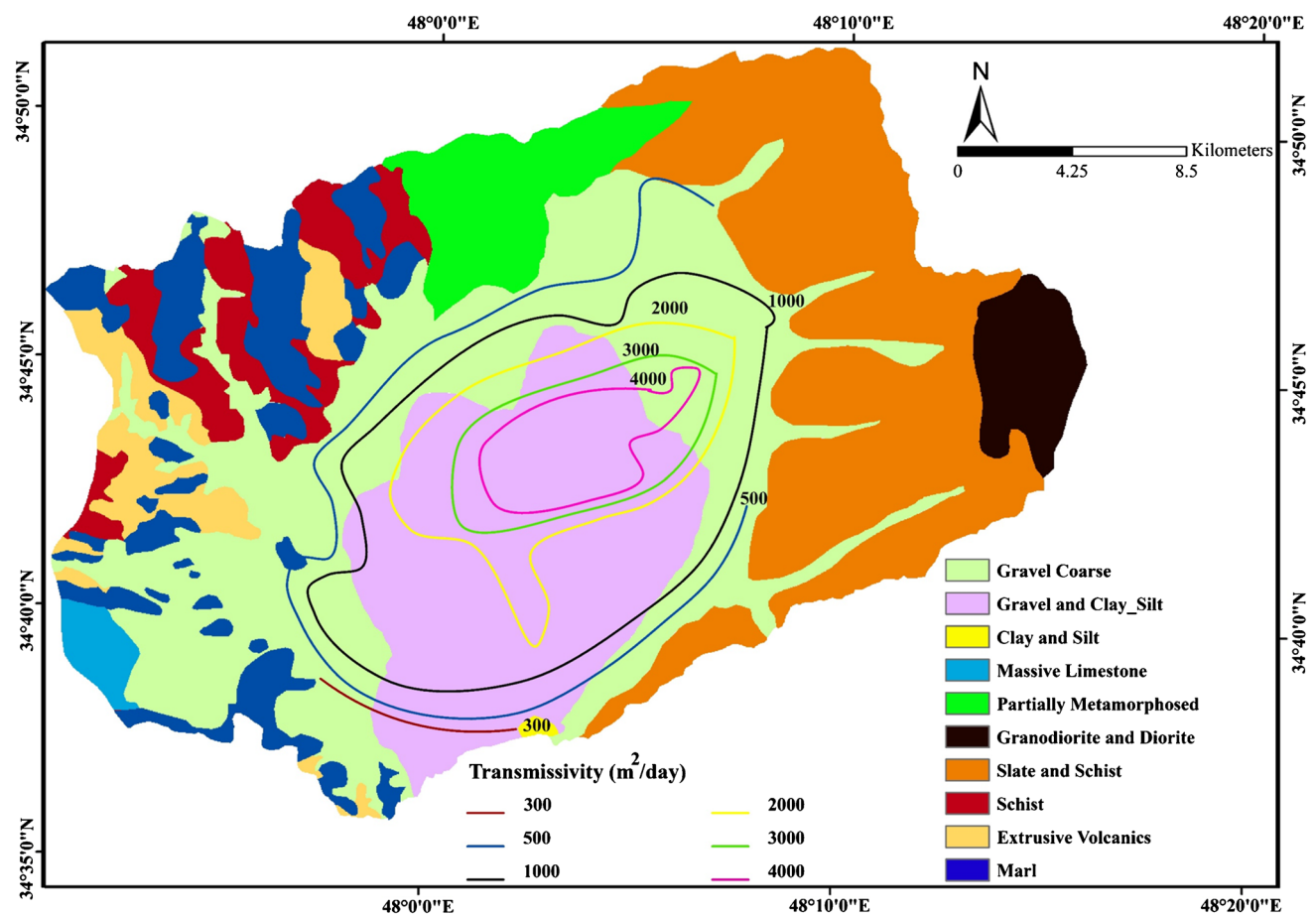


Fig. 19 Transmissivity (m²/day) map in the study area

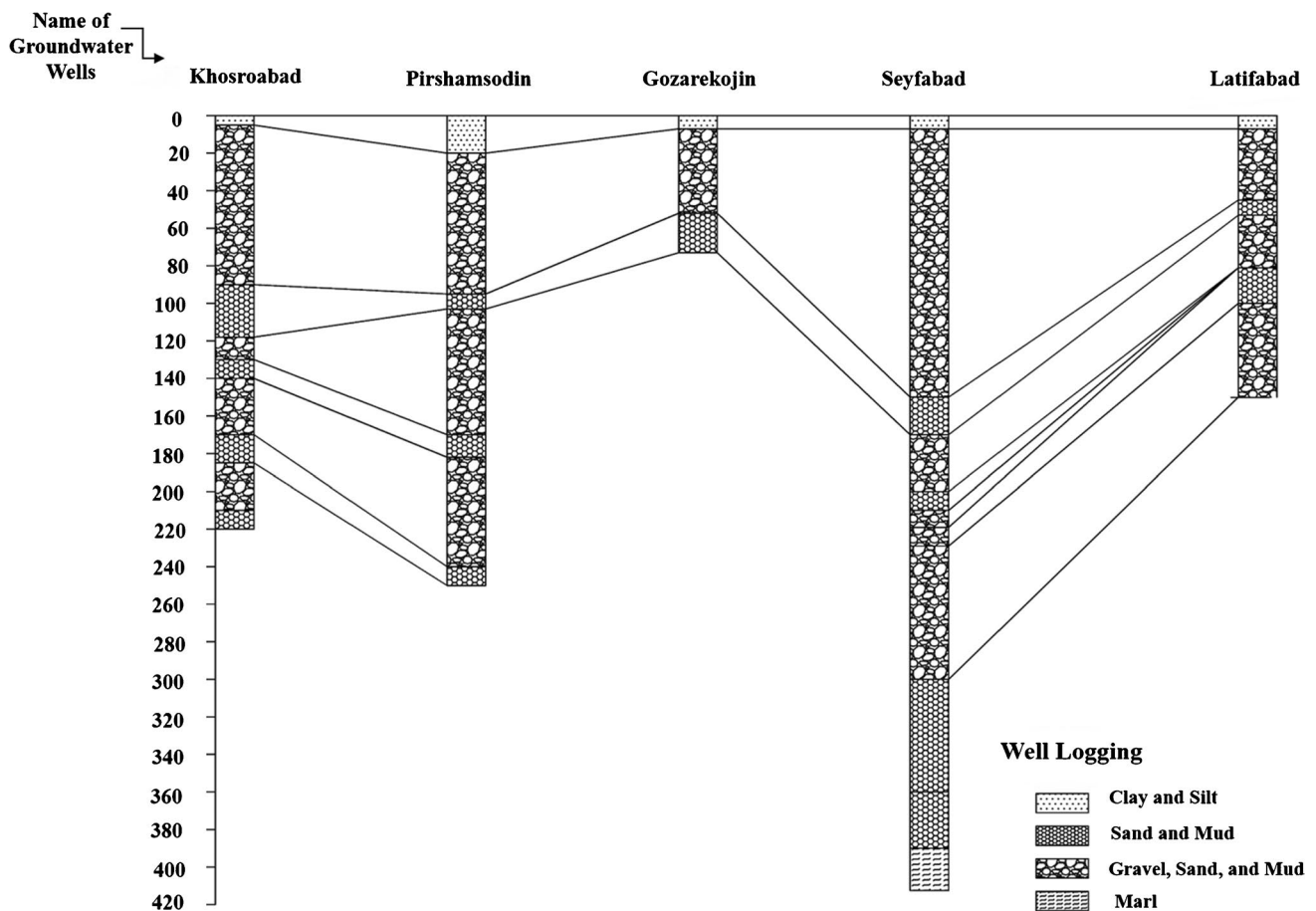


Fig. 20 Lithologs from exploration wells in the study area

in the Asadabad plain and geologic cross-sections can be used. Lithologs show that the surficial layer of clay and silt ranges from 1- to 20-m thick. The maximum thickness of silt was observed only at Pirshamsodin well. The second layer, which has been observed in all exploratory wells in the Asadabad plain, has a higher sand and gravel content and ranges from 1 to 300 m thick. The results of VES and lithologs also show that fine-grained sediments 80- to 120-m thick with undulating nature overlie coarse-grained sediments in the center of the plain, thus forming a semi-confined to the confined aquifer (Fig. 20). The defined sand to clay ratio by Rusydy et al. (2020) has made a quick method to assess the suitable area for digging wells, interpreting rich shallow depth to groundwater. The observation in boreholes (Fig. 20) shows that the mentioned ratio approaches more than 0.7 at the central part of the Asadabad plain, reflecting easier access to groundwater resources in the region.

Conclusions

The combination of GIS and RS was used to determine groundwater potential in the Asadabad plain in Hamadan province (Iran). Eleven parameters (rainfall, lithology,

drainage density, lineament density, land use, topography, slope, slope aspect, distance from stream, distance from lineaments, and air temperature) with weights selected using AHP were used to prepare the final groundwater potential map. In general, the central areas of the plain have high groundwater potential. Furthermore, VES was used to prepare a transverse resistance map, which is in good agreement with the groundwater potential map using the combined method. Both maps were validated with water-level and lithologic data collected in the plain, which shows the acceptable accuracy of the results in this study. The final groundwater potential map is a useful tool for local authorities and water managers in selecting sites for drilling new water wells. Groundwater quality was not taken into account in this study, so polluted areas are excluded from the final map. Nevertheless, the flexibility of the method enables the addition of parameters related to vulnerability to pollution and water-quality characteristics. Furthermore, the revision of the weights of included parameters is possible in future research. Finally, the applied method would benefit from simulation of the water cycle in the study area, using computer modeling and isotope analysis, as well as from more drilling data.

Declarations

Conflict of interest The authors declare no competing interests.

References

- Abdalla F (2012) Mapping of groundwater prospective zones using remote sensing and GIS techniques: a case study from the Central Eastern Desert, Egypt. *J Afr Earth Sci* 70:8–17. <https://doi.org/10.1016/j.jafrearsci.2012.05.003>
- Abuzied SM, Kaiser MF, Shendi EAH, Abdel-Fattah MI (2020) Multi-criteria decision support for geothermal resources exploration based on remote sensing, GIS and geophysical techniques along the Gulf of Suez coastal area, Egypt. *Geothermics* 88:101893. <https://doi.org/10.1016/j.geothermics.2020.101893>
- Al-Abadi AM, Shahid S (2015) A comparison between index of entropy and catastrophe theory methods for mapping groundwater potential in an arid region. *Environ Monit Assess* 187(9):1–21. <https://doi.org/10.1007/s10661-015-4801-2>
- Al-Abadi AM, Al-Temmeme AA, Al-Ghanimy MA (2016) A GIS-based combining of frequency ratio and index of entropy approaches for mapping groundwater availability zones at Badra–Al Al-Gharbi–Teeb areas, Iraq. *Sustain Water Resour Manag* 2(3):265–283. <https://doi.org/10.1007/s40899-016-0056-5>
- Antonakos AK, Voudouris KS, Lambrakis NI (2014) Site selection for drinking-water pumping boreholes using a fuzzy spatial decision support system in the Korinthia prefecture, SE Greece. *Hydrogeol J* 22(8):1763–1776. <https://doi.org/10.1007/s10040-014-1166-5>
- Arulbalaji P, Padmalal D, Sreelash K (2019) GIS and AHP techniques based delineation of groundwater potential zones: a case study from southern Western Ghats, India. *Sci Rep* 9(1):1–17
- Bagheri D (2017) Application of remote sensing, geoelectrical and GIS in the evaluation of groundwater potential, Asadabad Basin, Hamadan. Bu-Ali Sina University, Iran Msc dissertation, (In Persian)
- Bhattacharya PK, Patra HP (1968) Direct Current Geoelectric Sounding. In: *Methods in Geochemistry and Geophysics*. Elsevier Company, Amsterdam/London/ New York
- Bobachev C (2002) IPI2Win: A windows software for an automatic interpretation of resistivity sounding data. PhD Dissertation, Moscow State University, Moscow
- Boulourchi MH (1979) Explanatory text of Kabudar Ahang quadrangle map. Geological and Mineral Survey of Iran, Tehran
- Bouwer H (1978) *Groundwater Hydrology*. McGraw-Hill Book, New York
- Braud J (1970) Les formations du Zagros dans la region de Kermanshah, Iran. *Bull Soc Geol Fr* 13(3-4):416–419
- Chen W, Panahi M, Khosravi K, Pourghasemi HR, Rezaie F, Parvinnezhad D (2019) Spatial prediction of groundwater potentiality using ANFIS ensembled with teaching-learning-based and biogeography-based optimization. *J Hydrol* 572:435–448. <https://doi.org/10.1016/j.jhydrol.2019.03.013>
- De Martonne E (1923) Aridité et indices d'aridité. *Acad des Sci Comptes Rendus* 182(23):1935–1938 (in French)
- Döll P, Lehner B, Kaspar F (2002) Global modeling of groundwater recharge. In: *Proceedings of 3rd International Conference on Water Resources and the Environment Research*. Technical University of Dresden, Dresden, pp 27–33
- Doolittle JA, Jenkinson B, Hopkins D, Ulmer M, Tuttle W (2006) Hydrogeological investigations with ground-penetrating radar (GPR): estimating water-table depths and local ground-water flow pattern in areas of coarse-textured soils. *Geoderma* 131(3-4):317–329. <https://doi.org/10.1016/j.geoderma.2005.03.027>
- Elewa HH, Qaddah AA (2011) Groundwater potentiality mapping in the Sinai Peninsula, Egypt, using remote sensing and GIS-water-shed-based modeling. *Hydrogeol J* 19(3):613–628. <https://doi.org/10.1007/s10040-011-0703-8>
- Eslamian S, Okhravi S, Eslamian F (2014) Groundwater-surface water interactions. In: Eslamian S (ed) *Handbook of Engineering Hydrology*. CRC Press, Boca Raton, pp 259–287
- Ganapuram S, Kumar GV, Krishna IM, Kahya E, Demirel MC (2009) Mapping of groundwater potential zones in the Musi basin using remote sensing data and GIS. *Adv Eng Softw* 40(7):506–518. <https://doi.org/10.1016/j.advengsoft.2008.10.001>
- Huan H, Wang J, Teng Y (2012) Assessment and validation of groundwater vulnerability to nitrate based on a modified DRASTIC model: a case study in Jilin City of northeast China. *Sci Total Environ* 440:14–23. <https://doi.org/10.1016/j.scitotenv.2012.08.037>
- Huber H (1953) Geological report on the upper Qarachai area between Saveh and Hamedan. Iranian Oil Company Geological Report, Tehran
- Iran Water Resources Management Company (2004) Study of Groundwater Resources in Assadabad Plain-Geological Report. Hamadan Regional Water Institute, Hamadan (In Persian)
- Jhariya DC, Khan R, Mondal KC, Kumar T, Singh VK (2021) Assessment of groundwater potential zone using GIS-based multi-influencing factor (MIF), multi-criteria decision analysis (MCDA) and electrical resistivity survey techniques in Raipur city, Chhattisgarh, India. *AQUA-Water Infrastruct Ecosyst Soc* 70(3):375–400
- Kazakis N (2018) Delineation of suitable zones for the application of managed aquifer recharge (MAR) in coastal aquifers using quantitative parameters and the analytical hierarchy process. *Water* 10(6):804. <https://doi.org/10.3390/w10060804>
- Kazakis N, Voudouris KS (2015) Groundwater vulnerability and pollution risk assessment of porous aquifers to nitrate: Modifying the DRASTIC method using quantitative parameters. *J Hydrol* 525:13–25. <https://doi.org/10.1016/j.jhydrol.2015.03.035>
- Keller GV, Friscknecht FC (1966) *Electrical method in geophysical Prospecting*. Pergamon press, Oxford
- Lambot S, Binley A, Slob E, Hubbard S (2008) Ground penetrating radar in hydrogeophysics. *Vadose Zone J* 7(1):137–139. <https://doi.org/10.2136/vzj2007.0180>
- Liu KF, Wu YH, Huang MC (2007) Detecting groundwater level in shallow unconfined aquifer with microwaves for use in debris flow warning. In: *Debris-Flow Hazards Mitigation: Mechanics, Prediction, and Assessment*. Millpress, Rotterdam
- Machiwal D, Jha MK, Mal BC (2011) Assessment of groundwater potential in a semi-arid region of India using remote sensing, GIS and MCDM techniques. *Water Resour Manag* 25(5):1359–1386. <https://doi.org/10.1007/s11269-010-9749-y>
- Mainoo PA, Manu E, Yidana SM, Agyekum WA, Stigter T, Duah AA, Preko K (2019) Application of 2D-Electrical resistivity tomography in delineating groundwater potential zones: case study from the voltaian super group of Ghana. *J Afr Earth Sci* 160:103618. <https://doi.org/10.1016/j.jafrearsci.2019.103618>
- Malczewski J (1999) *GIS and multicriteria decision analysis*. Wiley, New York
- Nagarajan M, Singh S (2009) Assessment of groundwater potential zones using GIS technique. *J Indian Soc Remote Sens* 37(1):69–77. <https://doi.org/10.1007/s12524-009-0012-z>
- Naghbi SA, Moghaddam DD, Kalantar B, Pradhan B, Kisi O (2017) A comparative assessment of GIS-based data mining models and a novel ensemble model in groundwater well potential mapping. *J Hydrol* 548:471–483. <https://doi.org/10.1016/j.jhydrol.2017.03.020>
- Narany TS, Ramli MF, Fakharian K, Aris AZ (2016) A GIS-index integration approach to groundwater suitability zoning for irrigation

- purposes. Arab J Geosci 9(7):1–15. <https://doi.org/10.1007/s12517-016-2520-9>
- Nejad HT, Mumipour M, Kaboli R, Najib OA (2011) Vertical electrical sounding (VES) resistivity survey technique to explore groundwater in an arid region, Southeast Iran. J Appl Sci 11(23):3765–3774. <https://doi.org/10.3923/jas.2011.3765.3774>
- Oikonomidis D, Dimogianni S, Kazakis N, Voudouris K (2015) A GIS/remote sensing-based methodology for groundwater potentiality assessment in Tirnavos area, Greece. J Hydrol 525:197–208. <https://doi.org/10.1016/j.jhydrol.2015.03.056>
- Park I, Kim Y, Lee S (2014) Groundwater productivity potential mapping using evidential belief function. Groundwater 52(S1):201–207. <https://doi.org/10.1111/gwat.12197>
- Pourghasemi HR, Pradhan B, Gokceoglu C (2012) Application of fuzzy logic and analytical hierarchy process (AHP) to landslide susceptibility mapping at Haraz watershed, Iran. Nat Hazards 63(2):965–996. <https://doi.org/10.1007/s11069-012-0217-2>
- Rahmati O, Samani AN, Mahdavi M, Pourghasemi HR, Zeinivand H (2015) Groundwater potential mapping at Kurdistan region of Iran using analytic hierarchy process and GIS, Arab. J Geosci 8(9):7059–7071. <https://doi.org/10.1007/s12517-014-1668-4>
- Rajkumar S, Srinivas Y, Nair NC, Arunbose S (2019) Groundwater quality and vertical electrical sounding data of the Valliyar River Basin, South West Coast of Tamil Nadu, India. Data brief 24:103919. <https://doi.org/10.1016/j.dib.2019.103919>
- Rusyd I, Setiawan B, Idris S, Basyar K, Putra YA (2020) Integration of borehole and vertical electrical sounding data to characterise the sedimentation process and groundwater in Krueng Aceh basin, Indonesia. Groundw Sustain Dev 10:100372. <https://doi.org/10.1016/j.gsd.2020.100372>
- Saaty TL (1980) The Analytic Hierarchy Process. McGraw Hill, New York
- Samouëlian A, Cousin I, Richard G, Tabbagh A, Bruand A (2003) Electrical resistivity imaging for detecting soil cracking at the centimetric scale. Soil Sci Soc Am J 67(5):1319–1326. <https://doi.org/10.2136/sssaj2003.1319>
- Saraf AK, Choudhury PR (1998) Integrated remote sensing and GIS for groundwater exploration and identification of artificial recharge sites. Int J Remote Sens 19(10):1825–1841. <https://doi.org/10.1080/014311698215018>
- Sener E, Davraz A, Ozcelik M (2005) An integration of GIS and remote sensing in groundwater investigations: a case study in Burdur, Turkey. Hydrogeol J 13(5-6):826–834. <https://doi.org/10.1007/s10040-004-0378-5>
- Song SH, Lee JY, Park N (2007) Use of vertical electrical soundings to delineate seawater intrusion in a coastal area of Byunsan, Korea. Environ Geol 52(6):1207–1219. <https://doi.org/10.1007/s00254-006-0559-8>
- Song L, Zhu J, Yan Q, Kang H (2012) Estimation of groundwater levels with vertical electrical sounding in the semiarid area of South Keerqin sandy aquifer, China. J Appl Geophys 83:11–18. <https://doi.org/10.1016/j.jappgeo.2012.03.011>
- Sudduth KA, Kitchen NR, Bollero GA, Bullock DG, Wiebold WJ (2003) Comparison of electromagnetic induction and direct sensing of soil electrical conductivity. Agron J 95(3):472–482. <https://doi.org/10.2134/agronj2003.4720>
- Tizro AT (2002) Hydrogeological investigations by surface geoelectrical method in hard rock formation- a case study. Geological Society of Malaysia Annual Geological Conference, Kelantan
- Tizro AT, Voudouris KS, Salehzade M, Mashayekhi H (2010) Hydrogeological framework and estimation of aquifer hydraulic parameters using geoelectrical data: a case study from West Iran. Hydrogeol J 18(4):917–929. <https://doi.org/10.1007/s10040-010-0580-6>
- Tizro AT, Voudouris K, Basami Y (2012) Estimation of porosity and specific yield by application of geoelectrical method—a case study in western Iran. J Hydrol 454:160–172. <https://doi.org/10.1016/j.jhydrol.2012.06.009>
- Urish DW (1983) The practical application of surface electrical resistivity to detection of ground-water pollution. Groundwater 21(2):144–152. <https://doi.org/10.1111/j.1745-6584.1983.tb00711.x>
- Voudouris K, Kazakis N, Polemio M, Kareklas K (2010) Assessment of intrinsic vulnerability using DRASTIC model and GIS in Kiti aquifer, Cyprus. Eur Water 30:13–24
- White PA (1994) Electrode arrays for measuring groundwater flow direction and velocity. Geophysics 59(2):192–201. <https://doi.org/10.1190/1.1443581>
- Younis A, Osman OM, Khalil AE, Nawawi M, Soliman M, Tarabees EA (2019) Assessment groundwater occurrences using VES/TEM techniques at North Galala plateau, NW Gulf of Suez, Egypt. J Afr Earth Sci 160:103613. <https://doi.org/10.1016/j.jafrearsci.2019.103613>
- Zohdy AAR (1989) A new method for the automatic interpretation of Schlumberger and Wenner sounding curves. Geophysics 54(2):245–253. <https://doi.org/10.1190/1.1442648>
- Zohdy AAR, Eaton GP, Mabey DR (1974) Application of surface geophysics to groundwater investigations. In: US Geological Survey. USGS-TWRI, Reston
- Springer Nature or its licensor holds exclusive rights to this article under a publishing agreement with the author(s) or other rightsholder(s); author self-archiving of the accepted manuscript version of this article is solely governed by the terms of such publishing agreement and applicable law.